Geophysical Research Letters *Explore this journal >*

View issue TOC
Volume 34, Issue 15
August 2007

Climate

Cloud and radiation budget changes associated with tropical intraseasonal oscillations

Roy W. Spencer, William D. Braswell, John R. Christy, Justin Hnilo

First published:
9 August 2007 Full publication history

DOI:
10.1029/2007GL029698 View/save citation

Abstract

[1] We explore the daily evolution of tropical intraseasonal oscillations in satellite-observed tropospheric temperature, precipitation, radiative fluxes, and cloud properties. The warm/rainy phase of a composited average of fifteen oscillations is accompanied by a net reduction in radiative input into the ocean-atmosphere system, with longwave heating anomalies transitioning to longwave cooling during the rainy phase. The increase in longwave cooling is traced to decreasing coverage by ice clouds, potentially supporting Lindzen's “infrared iris” hypothesis of climate

1. Introduction

[2] The tropical tropospheric heat budget is dominated by a quasi-equilibrium balance between latent heating in precipitation systems and longwave (infrared) cooling to outer space [e.g., *Manabe and Strickler*, 1964]. The precipitation systems also produce clouds that both warm the atmosphere through longwave "greenhouse" warming, and cool the surface through shortwave (solar) shading.

[3] While many investigators have found that these two cloud effects mostly cancel in their influence on the tropical ocean-atmosphere system's heat budget [e.g., *Kiehl and Ramanathan*, 1990; *Cess et al.*, 2001], any imbalance between these two large terms could significantly feed back on global warming [*Chou and Lindzen*, 2002; *Soden and Held*, 2006]. This makes accurate convective and cloud parameterizations in General Circulation Models (GCMs) critical for improving confidence in those model's predictions of future warming.

[4] *Aires and Rossow* [2003] and *Stephens* [2005] argue that substantial improvements in GCM parameterizations will not be achieved by inferring "feedbacks" from observed monthly, interannual, or even decadal climate variability. Partly because of the difficulty in separating cause and effect in observational data, they recommend the measurement of high time-resolution (e.g., daily) variations in the relationships (sensitivities) between clouds, radiation, temperature, etc., which can then be compared to the same metrics diagnosed from GCMs.

[5] Here we address the observational part of this recommendation by analyzing the daily evolution of a time composite of fifteen tropical intraseasonal oscillations (ISOs) in a variety of satellite-measured variables. While most investigations of these events examine their regional expression over the tropical west Pacific [e.g., *Stephens et al.*, 2004], we will instead analyze larger-scale, tropical oceanic averages in an attempt to better capture both ascending and descending branches of tropical deep convective circulations and hopefully better estimate their net effect on the tropical atmosphere.

2. Data and Analysis Method

[6] Tropical (20°N to 20°S latitude) oceanic averages covering the period 1 March 2000 to 31 December 2005 were analyzed. Tropospheric air temperature estimates (T_a) come from channel 5 of the Advanced Microwave Sounding Unit (AMSU-A) flying on the NOAA-15 polar orbiting satellite (instrument descriptions can be found at http://www2.ncdc.noaa.gov/docs/klm/html/c1/sec1-1.htm). AMSU channel 5 (53.596 GHz) measurements approximate the average temperature of a deep layer of the troposphere, with peak sensitivity around 600 mb. There is a small, 4% to 5%, influence on channel 5 from the tropical lower stratosphere and about a 1% contribution from the ocean surface.

[7] Tropical oceanic measurements of rainfall, surface wind speed, total integrated water vapor, and sea surface temperature (SST) come from NASA's Tropical Rainfall Measuring Mission (TRMM)

satellite Microwave Imager (TMI), described by ***Kummerow et al.* [1998]** . The TMI rainfall algorithm is described by ***Wentz and Spencer* [1998]** , while the non-rainfall products are described by ***Wentz* [1997]** and ***Wentz et al.* [2000]** .

[8] Top of the atmosphere (TOA), all-sky and clear-sky outgoing longwave (LW) and reflected shortwave (SW) flux measurements were made by the Terra satellite Clouds and the Earth's Radiant Energy System (CERES) instrument [***Wielicki et al.*, 1996**]. These products, taken from the CERES ES4 Terra FM1 Edition 2 dataset, are “ERBE-like”, and are meant to provide continuity with NASA's older Earth Radiation Budget Experiment satellite. We applied the “Rev. 1” corrections, reported by the data provider, to the SW data.

[9] Finally, cloud properties are from the Terra Moderate Resolution Imaging Spectroradiometer (MODIS) [***Barnes et al.*, 1998**], using the latest daily Collection 5 MOD08_D3 dataset. All of the original product datasets are daily grids, at either 1.0° or 2.5° spatial resolution, except for the TMI products which are three-day grids compiled on a daily basis at 0.25° spatial resolution. The AMSU grids of limb-corrected T_a [***Spencer and Braswell*, 1997**] are archived in-house at UAH as part of our monthly routine processing of global tropospheric temperatures [***Christy et al.*, 2003**].

[10] We averaged all daily grids into daily zonal averages for the latitude band 20°N to 20°S, oceans only. Any days with less than 80% of the nominal data coverage were interpolated from the surrounding days' averages. All results that follow are for daily anomalies, which were computed by subtracting a 21-day smoothed average annual cycle from the six year time series of daily zonal averages.

[11] From the daily anomalies, we constructed a time-composite of the fifteen strongest ISOs during the six year period of record, requiring each to be at least 40 days from temperature minimum to temperature minimum. Table 1 lists the dates of maximum T_a about which the ISOs were composited. As an example of the ISO signature, Figure 1 shows two satellites' measurements of daily T_a during 2002. The stronger oscillations have about a 40 day time scale, which is typical of these disturbances [e.g., ***Madden and Julian*, 1994**].

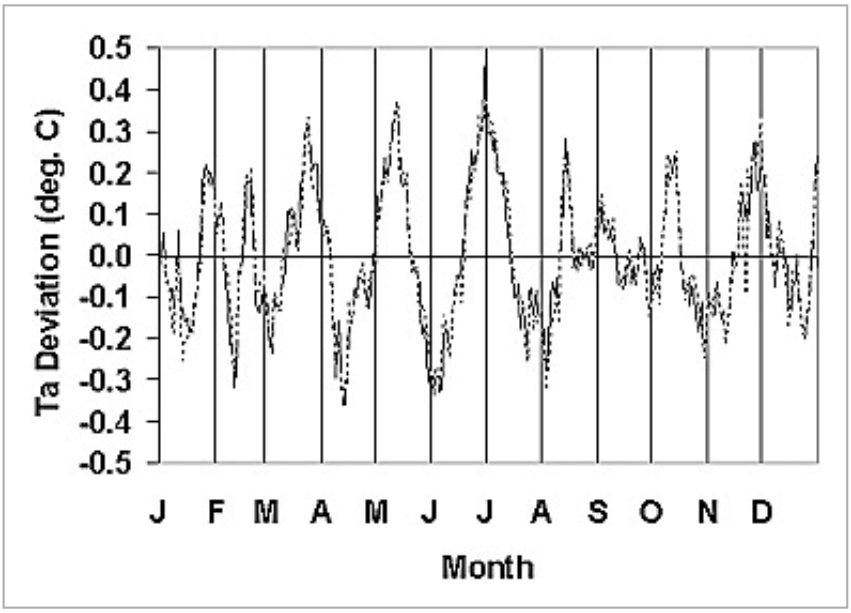

Figure 1.

Open in figure viewer

One year of daily tropical average tropospheric temperature from AMSU channel 5 during 2002, solid line is NOAA-15 and dotted line is NOAA-16 satellite. The time series has been high pass filtered to remove time variations longer than intraseasonal.

Table 1. Dates of Maximum Tropospheric Temperature Anomaly in AMSU Channel 5 for Fifteen ISO Events Chosen for Composite Analysis[a]

ISO Event	Date of Peak Tropospheric Temperature (T_a)
1	(1 September 2000)
2	12 February 2001
3	4 May 2001
4	(1 July 2001)
5	18 August 2001
6	(24 March 2002)
7	12 May 2002
8	30 June 2002
9	(11 May 2004)
10	(14 June 2004)
11	(18 August 2004)
12	28 February 2005
13	12 June 2005
14	25 July 2005
15	7 September 2005

a Dates in parentheses correspond to ISOs that did not have sufficient data to be included in the composite analysis of MODIS cloud properties.

3. ISO Signals

[12] The composite ISO signatures in T_a, oceanic surface wind speed, integrated water vapor, and SST (Figure 2a) reveal an increase in surface wind speed and water vapor, and a brief but weak warm signal in SST, during the ISO warming phase. The wind speed and water vapor increases imply enhanced oceanic evaporation rates. During the cooling phase, wind speeds and vapor contents decrease. The amplitude of the wind signal is 15% of the tropical average wind speed, while that of the water vapor oscillation is only 1.5% of its average value.

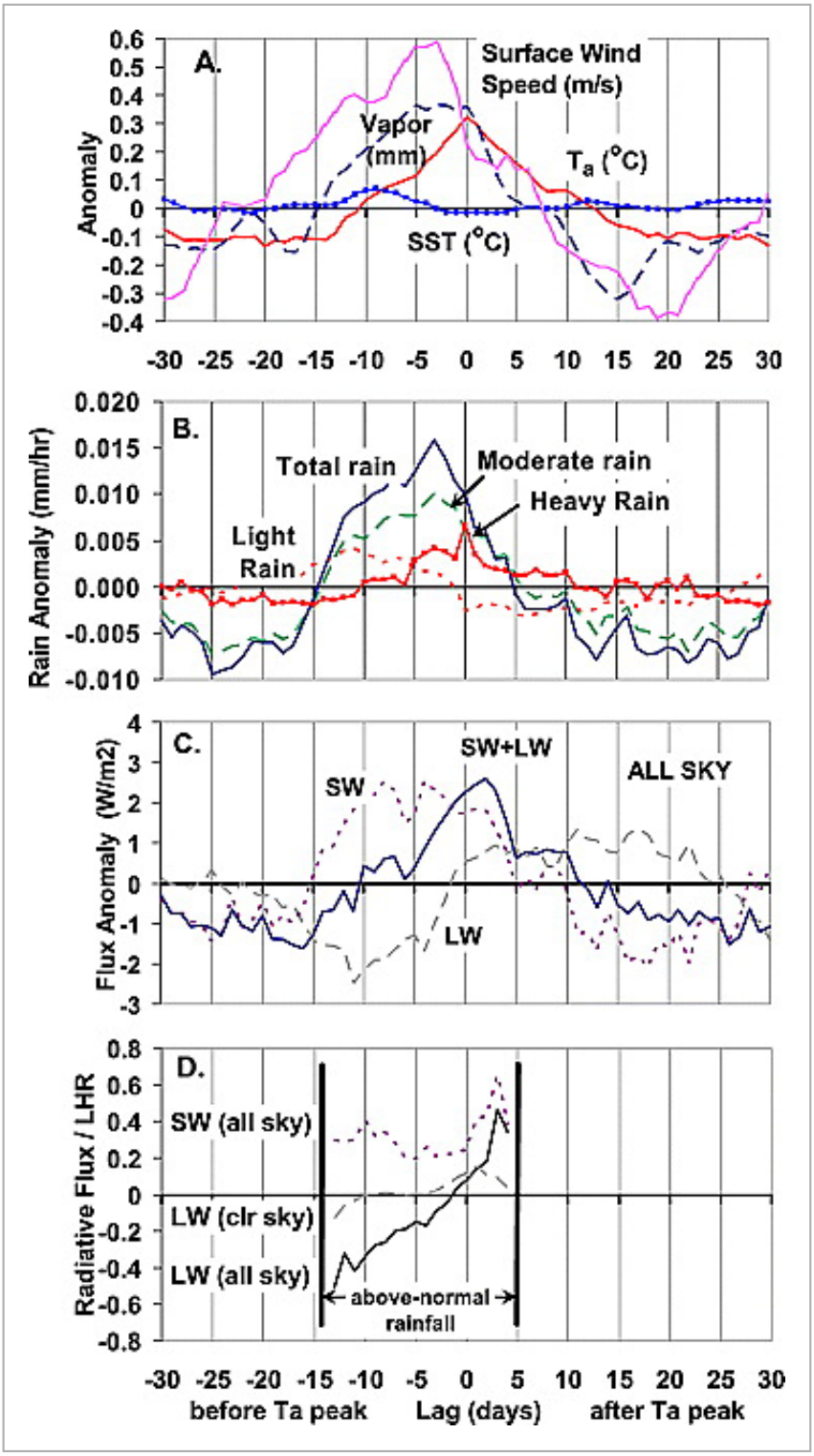

Figure 2.

Open in figure viewer

Composite analysis of daily zonal average oceanic anomalies (20°N to 20°S) associated with 15 ISOs, relative to the date of peak tropospheric temperature (T_a): (a) AMSU T_a, and surface wind speed, integrated water vapor, and SST from the TRMM TMI; (b) TMI rain rate; (c): CERES all-sky top-of-atmosphere outgoing longwave (*LW*) and reflected shortwave (*SW*) fluxes; (d) CERES fluxes divided by latent heat release calculated from "total rainfall" in Figure 2b.

[13] Most of the above-average rainfall occurs during the T_a warming phase (Figure 2b), with an oscillation amplitude about 20% of the mean rain rate, and a shift in the rain rate distribution to heavier rates during the rainy phase of the oscillation.

[14] Variations in the CERES TOA all-sky (cloudy plus clear) SW and LW fluxes (Figure 2c) reveal the expected increase in reflected SW flux associated with clouds produced by the rain systems. But the transition from negative to positive LW flux anomalies during the period of above-average rainfall is somewhat surprising. To examine how these flux variations relate to rainfall variations, we divided the radiative flux anomalies by the latent heat release anomalies calculated from the "total rain" curve in Figure 2b. The results (Figure 2d) reveal the usual near-cancellation between LW heating and SW cooling, but only early in the ISO rainy phase. The LW anomalies then unexpectedly transition from warming to cooling during the course of the rainy period. That the all-sky LW change is so much larger than the clear-sky LW change suggests a shift in cloud properties, which brings us to the MODIS cloud product analysis.

[15] Due to an incomplete MODIS data record, all anomalies were recomputed using nine of the original fifteen ISOs for which there were MODIS data available (see Table 1). The resulting composite T_a anomaly (Figure 3a) has a signature very similar to that of the fifteen-ISO composite in Figure 2a. The MODIS cloud products revealed three significant changes associated with the ISO. First, the liquid cloud coverage (Figure 3b) approximately follows the rain activity variations seen in Figure 2a and the reflected SW variations in Figure 2c, but with a likely under estimation between lag days −15 to 0 due to obscuration by overlying ice clouds.

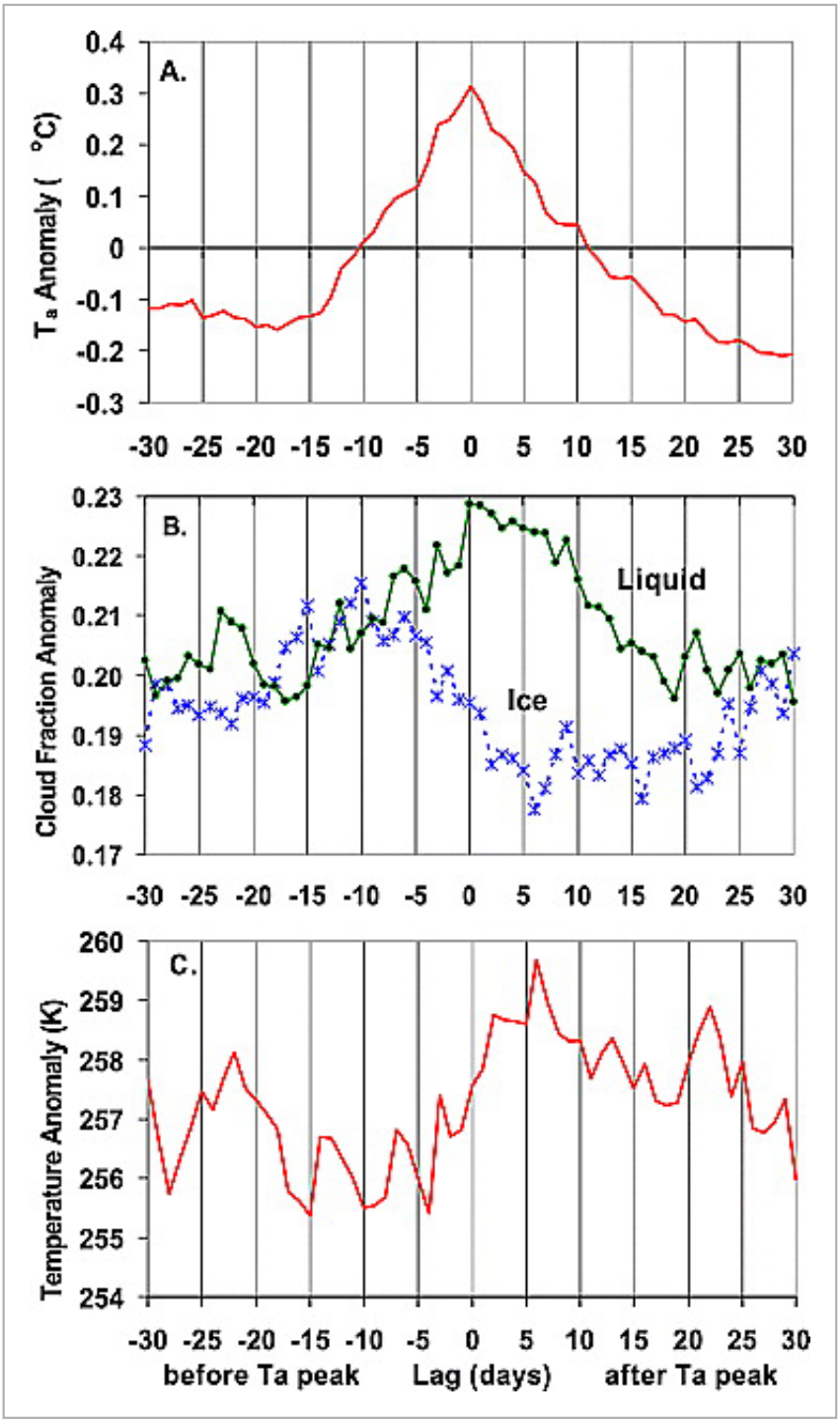

Figure 3.

Open in figure viewer

As in Figure 2 but for a composite of nine ISO's: (a) tropospheric temperature, (b) MODIS liquid and ice cloud fractions, and (c) cloud top temperature (all clouds). The tropical average cloud fraction and cloud top temperature have been added to the anomalies in Figures 3b and 3c.

[16] Of greater interest, however, is the ice cloud behavior, which has a much stronger influence on LW

fluxes than do liquid clouds. A decrease in ice cloud coverage is seen in Figure 3b, which coincides with the increasing LHR-normalized LW flux seen in Figure 2d. Finally, the average cloud top temperature of all (liquid + ice) clouds warms by 2°C to 3°C during the same period (Figure 3c). Since the cloud top temperature reported in the MODIS data product we used is an average for all cloud types, this cloud top warming might simply be the result of the decreasing ice cloud fraction uncovering liquid clouds below. In any event, both of these changes in ice cloud properties are qualitatively consistent with the all-sky LW transition seen in Figures 2c and 2d.

[17] We estimated the potential effect of the MODIS-observed ice cloud fraction change on the LW flux from

$$\Delta LW = (f_2 - f_1)(LW_{ice} - LW_{no-ice}) \qquad (1)$$

where f_1 and f_2 are ice cloud fractions during the warming and cooling phases of the ISO, respectively; LW_{ice} is the ice cloud flux; and LW_{no-ice} is the flux from the remaining areas. With a MODIS-observed decrease in ice cloud fraction from 0.208 ten days before, to 0.184 ten days after the peak in T_a, and assuming average ice cloud and non-ice cloud LW fluxes of 200 and 285 W m^{-2} (respectively, that we estimated from frequency distributions of all CERES LW data), we estimate a LW flux increase of around 2.0 W m^{-2}. This is roughly consistent with the 2.5 W m^{-2} CERES-measured increase in LW flux seen in Figures 2c and 2d during the ISO rainy phase.

[18] The decrease in ice cloud coverage is conceptually consistent with the “infrared iris” hypothesized by ***Lindzen et al.*** **[2001]** , who proposed that tropical cirroform cloud coverage might open and close, like the iris of an eye, in response to anomalously warm or cool conditions, providing a negative radiative feedback on temperature change. We caution, though, that the ice cloud reduction with tropospheric warming reported here is on a time scale of weeks; it is not obvious whether similar behavior would occur on the longer time scales associated with global warming.

[19] We also computed the sensitivity relationships between T_a and the cloud portion of the SW and LW radiative fluxes, which should be of use for comparing to the high time resolution behavior exhibited by climate models. The cloud radiative forcing (CRF), can be been defined [e.g., ***Cess et al.*** **, 2001**] as:

$$SW\,CRF = -(SW_{all} - SW_{clr}) \qquad (2)$$

$$\text{and } LW\,CRF = -(LW_{all} - LW_{clr}), \qquad (3)$$

where the sign convention now changes so that positive values of CRF represent heating (flux input), and in our case all quantities are anomalies (deviations from average). The clear-sky SW anomalies (not shown) were small, and are believed to be due to residual cloud contamination in the ERBE methods for identifying clear sky (B. Wielicki, personal communication, 2007). Therefore, the all-sky SW will be assumed to also represent the SW cloud radiative forcing (SW CRF ≈ −SW_{all}). The clear sky LW anomalies (not shown) were also small (as can be gleaned from Figure 2d), but are still included in our computation of the LW CRF.

[20] The sum of SW CRF (≈−SW_{all}) and LW CRF(= −[LW_{all} − LW_{clr}]) plotted against the tropospheric temperature anomalies for the middle 41 days of the fifteen-ISO composite (Figure 4) reveals a strongly negative relationship. A linear regression yields a sensitivity factor (slope) of −6.1 W m^{-2} K^{-1},

with an explained variance of 85.0%. This indicates that the net (SW + LW) radiative effect of clouds during the evolution of the composite ISO is to cool the ocean-atmosphere system during its tropospheric warm phase, and to warm it during its cool phase.

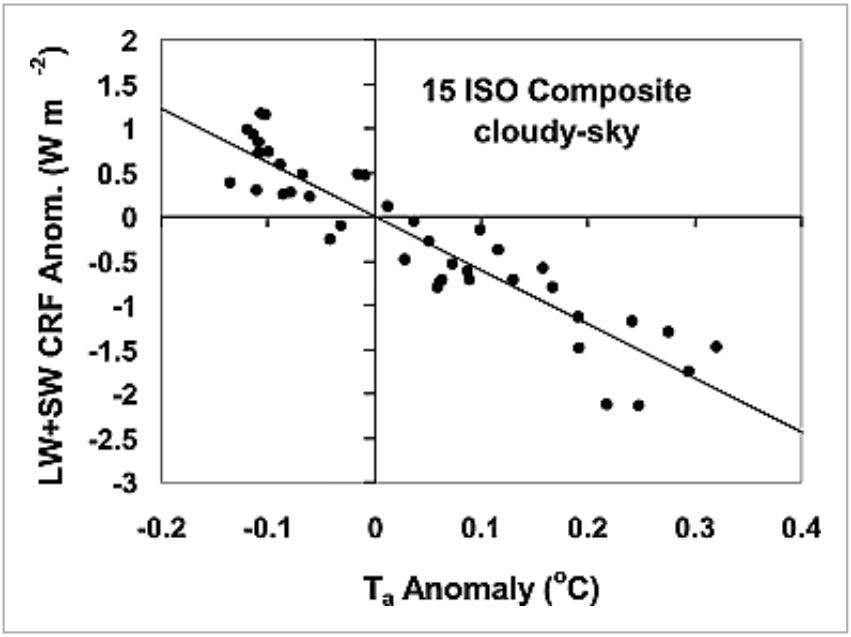

Figure 4.

Open in figure viewer

The sum of SW and LW cloud radiative forcings (CRF) versus tropospheric temperature for the 15-ISO composite, which represents about 30% of the six-year data record.

4. Discussion and Conclusions

[21] The composite of fifteen strong intraseasonal oscillations we examined revealed that enhanced radiative cooling of the ocean-atmosphere system occurs during the tropospheric warm phase of the oscillation. Our measured sensitivity of total (SW + LW) cloud radiative forcing to tropospheric temperature is −6.1 W m^{-2} K^{-1}. During the composite oscillation's rainy, tropospheric warming phase, the longwave flux anomalies unexpectedly transitioned from warming to cooling, behavior which was traced to a decrease in ice cloud coverage. This decrease in ice cloud coverage is nominally supportive of Lindzen's “infrared iris” hypothesis. While the time scales addressed here are short and not necessarily indicative of climate time scales, it must be remembered that all moist convective adjustment occurs on short time scales. Since these intraseasonal oscillations represent a dominant mode of convective variability in the tropical troposphere, their behavior should be considered when testing the convective and cloud parameterizations in climate models that are used to predict global warming.

Acknowledgments

[22] The TMI data products are produced by Remote Sensing Systems (available at www.remss.com) and are sponsored by the NASA Earth Science REASoN DISCOVER Project. The CERES data were obtained from the NASA Langley Research Center EOSDIS Distributed Active Archive Center. The MODIS data are available at http://ladsweb.nascom.nasa.gov/data/ftp_site.html. This research was supported by NOAA contract NA05NES4401001 and DOE contract DE-FG02-04ER63841. J. Hnilo was supported under the auspices of the DOE Office of Science, Climate Change Prediction Program by University of California Lawrence Livermore National Laboratory, contract W-7405-Eng-48.

Supporting Information

References

Citing Literature